DEVELOPMENT OF A CARGO AIRCRAFT, AN OVERVIEW OF THE PRELIMINARY AERODYNAMIC DESIGN PHASE

S. Tsach, S. Bauminger, M. Levin, D. Penn and T. Rubin
Engineering center
Israel Aircraft Industries (IAI)
Ben-Gurion Airport, Israel

Abstract

This paper summarizes the preliminary design activity of a new cargo aircraft, including aerodynamic design and wind tunnel tests. A new concept of a dedicated cargo aircraft was evaluated by IAI. The fuselage shape was optimized for standard cargo containers. The resulting cross section was fairly rectangular. Other design requirements were - high speed, good ground performance, low fuel consumption and competitive price. These were met by choosing high power turboprop engines and by designing simple and efficient high lift devices.

During the preliminary aerodynamic design phase two major aspects were emphasized:

1. *Drag and lift goals*
2. *Good handling qualities, considering the high engine power effects*

Nomenclature

Tc	=	Thrust/qS
q	=	$0.5\rho V^2$
S	=	Reference area
Vmc	=	minimum control speed
Clmax	=	Maximum lift coefficient

1 Introduction

The concept of a new cargo aircraft was raised within IAI in the early nineties. The main idea was to design a specialized aircraft capable of carrying standard size aviation containers. Total cargo weight was within the medium capacity range. It would be a dedicated transport without passenger accommodation. This approach would enable efficient fuselage volume usage, and faster loading and unloading. Both the aircraft's purchase price and its direct operating cost (DOC) would be competitively low.

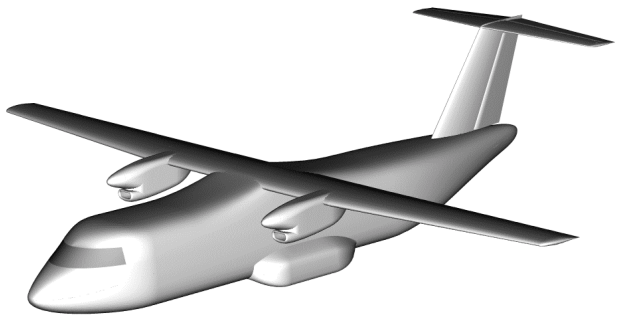

Figure 1: 3–D view of the cargo aircraft

A two engine turboprop aircraft was chosen as the best candidate. Volume efficiency was maximized by using a fairly rectangular fuselage cross section.

To prevent a possible obstruction to loading, a T–tail configuration was chosen [Figs. 1,2].

One of the principal goals of the aerodynamic work was to gain confidence in drag and lift levels, so that performance guarantees could be given to potential customers. Another goal was to evaluate stability and control, so that the configuration would meet civil certification requirements.

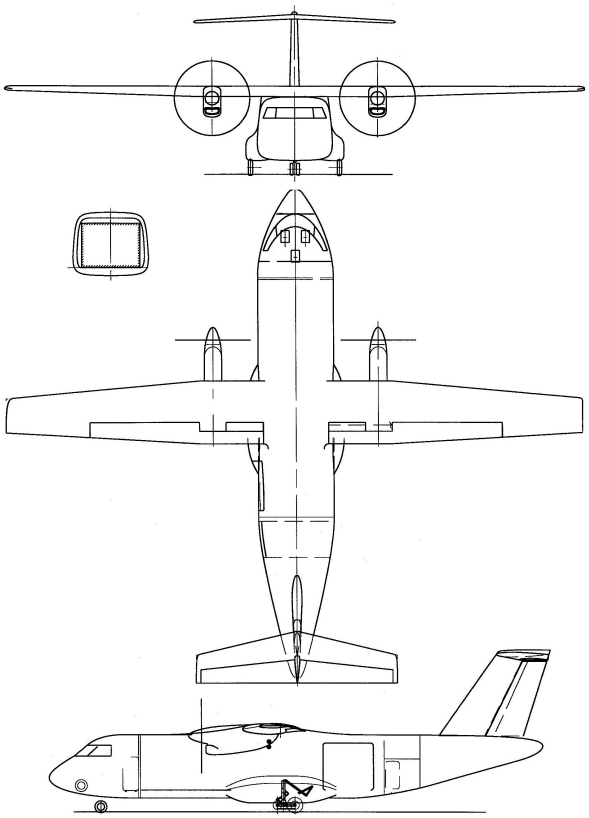

Figure 2: Views of configuration with a side-loading door

2 Wing Design

The main design point of the wings was to achieve low drag during cruise. The typical cruise conditions were Mach = 0.5, CL = 0.5, Reynolds number of about $2*10^7$ (root airfoil). The wing was assumed to be mostly turbulent in normal use due to the rough usage of the aircraft for cargo transport.

The second design point was derived from a requirement for short takeoff and landing. From the aerodynamic viewpoint this meant a requirement for high CLmax at low airspeeds. In weighing aerodynamic efficiency against price and complexity, a single slotted flap with a fixed hinge was chosen.

Thickness was required to be above 16% at root, due to structure and volume requirements.

A few known root airfoils were analyzed, and modifications were made in order to achieve design goals. The work was carried out using the MSES code [Ref. 1] and its associated inverse and optimization modules. The tip airfoil had a reduced thickness of about 13%. It was designed maintaining a rather high leading edge radius for higher Clmax.

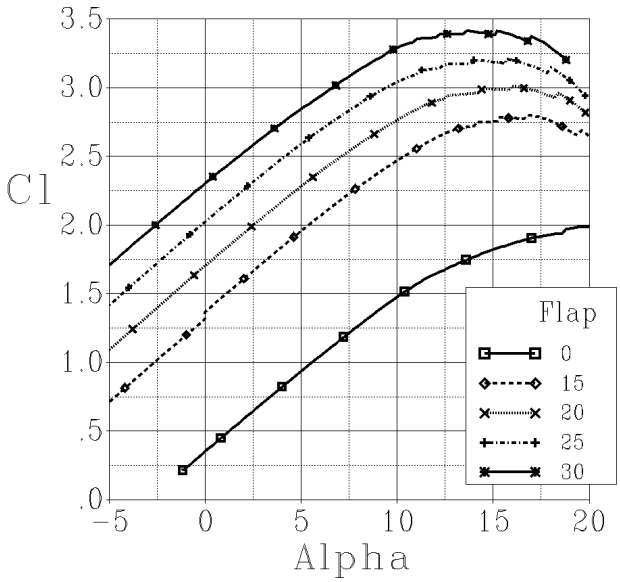

Figure 3: Flap deflection effect on root airfoil maximum lift, MSES computation, Mach=0.15, Reynolds=10^6, transition 5% upper, 40% lower

The calculated 2-D Clmax values for the root airfoil, with the simple slotted flap, were quite high [Fig. 3]. Since the code was assumed to overestimate the actual Clmax, the Clmax values that were used to predict aircraft performance were reduced by about 0.2.

The effect of Reynolds number on the maximum lift of the airfoils was computed [Fig. 4]. The main purpose was to use these calculations to correlate forthcoming wind tunnel test results with the full-scale aircraft predictions.

Drag level was computed assuming fully turbulent conditions [Fig. 5].

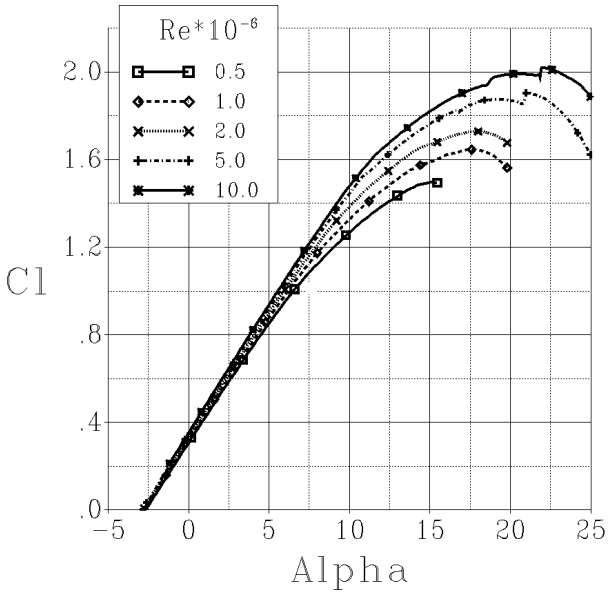

Figure 4: Reynolds number effect on predicted maximum lift of root airfoil, MSES, flap=0^0, Mach=0.15, transition 5% upper, 40% lower

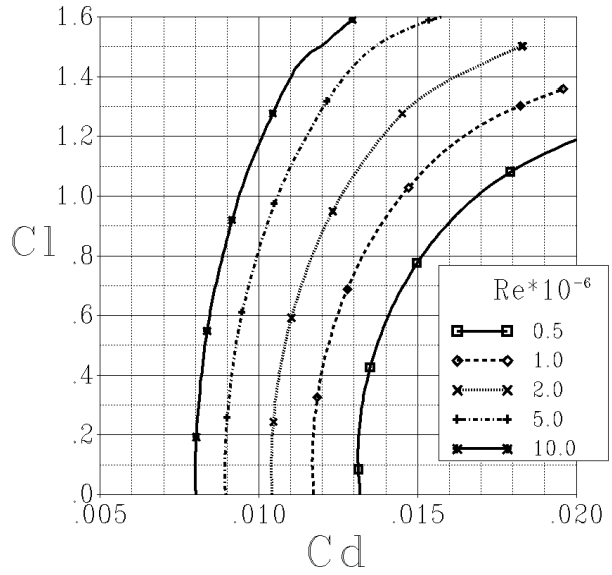

Figure 5: Reynolds number effect on predicted drag polar of root airfoil, MSES, flap=0^0, Mach=0.15, transition 5% upper and lower

The 3-D analysis of the wing was done with an Euler CFD code that was developed in IAI and AMI named MGAERO [2]. This unique code uses Cartesian grid blocks to facilitate input preparation. The analysis was done for several twist angles. The resulting wing spanwise loading was evaluated for both induced drag and for stall characteristics. Induced drag was not computed directly from the code but was rather estimated using lifting line theory and the computed spanwise loading. Stall characteristics and indication of maximum lift were checked by comparing spanwise local lift coefficient with predicted local maximum 2-D lift [Fig. 6]. A washout of 2^0 was chosen as an optimal design point.

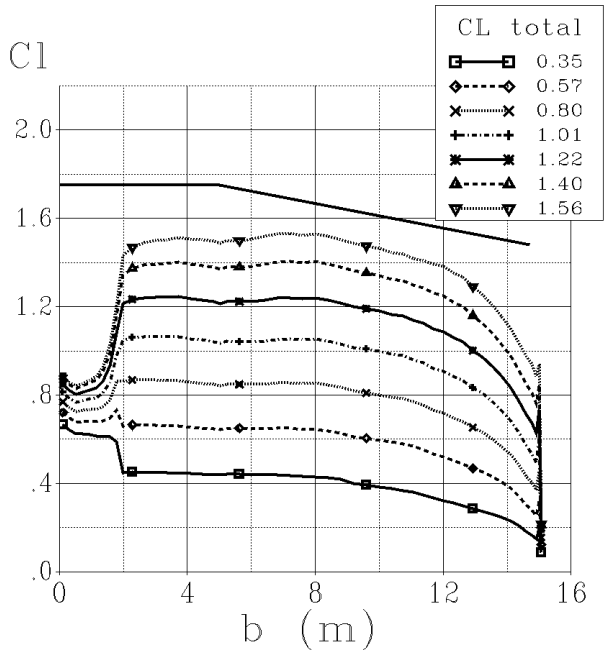

Figure 6: Wing local lift vs. span, MGAERO, flap=0^0, Mach=0.17, without nacelle and propeller. Upper curve is the predicted section Clmax at Reynolds=10^6

3 Drag and Lift

3.1 Rectangular cross section

Sources in literature [3], [4] indicated that the large rectangular fuselage cross section could cause a drag increase beyond standard fuselage shapes. A drag increase by a factor of about 1.25 compared to a circular body was considered possible. An effort was made to minimize the possibility of this drag by increasing the radius of the fuselage corners [Fig. 7].

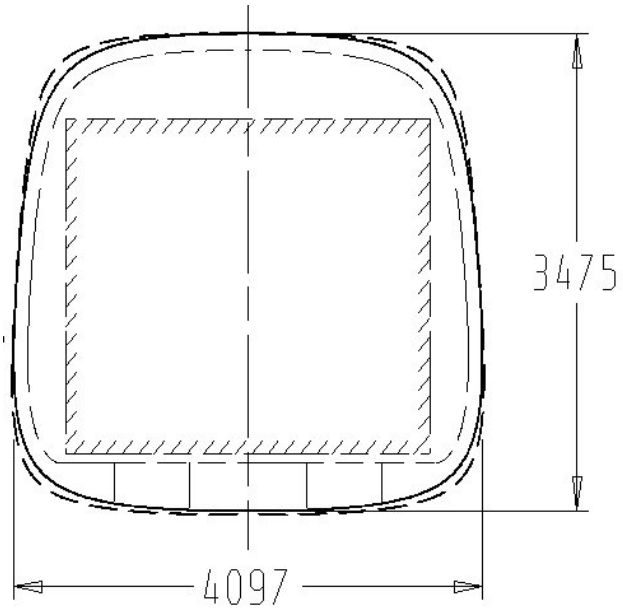

Figure 7: Body cross section evolution

3.2 Preliminary estimated drag polars

The drag polar of the aircraft was estimated for preliminary performance calculation. The drag of the fuselage was evaluated by a method for subsonic bodies [5], applying an additional factor of 1.25. The nacelles and tail drag was evaluated by an empirical method [5], [6]. Wing profile drag was computed by dividing it into strips, using the 2-D MSES code for calculating airfoil drag at each strip. The induced drag of the wing was computed as previously described. It was estimated that the wing-mounted propellers would change the lift distribution and cause an adverse effect on the induced drag efficiency. Therefore a lower value of induced drag efficiency was used for performance calculations.

Trim drag was computed by adding 3 contributors: the wing and tail additional induced drag due to increased CL, and the projection of tail lift due to downwash.

Miscellaneous drag was added due to various predicted installations, gaps of control surfaces, rivets, and inaccuracies in manufacturing, etc.

The drag polar was recalculated for the wind tunnel model. The main differences in this calculation were the lower Reynolds number, no propeller effects, and no miscellaneous drag.

3.3 Comparison to wind tunnel results

A model of the aircraft, scale 1:10, was built and tested in the IAI low speed wind tunnel (LSWT) [Fig. 8]. The wind tunnel tests were conducted in three phases that included:

1. Basic tests – longitudinal and lateral.
2. Evaluating the impact of wind tunnel model mounting on the results.
3. Evaluation of aerodynamic fixes to issues detected in first series.

The drag measurements [Fig 9] indicated that a somewhat lower drag was measured than the one predicted for the wind tunnel model. This was true both for the total configuration and for the wing - body alone configuration.

Figure 8: Model installation in wind tunnel, 3 bayonets mounting

The second wind tunnel test was performed with central bayonets [Fig. 10]. This installation allowed the measurement of body alone drag. Preliminary results showed that the body had lower drag than predicted. It seems likely therefore, that the large corner radii have reduced the fuselage drag. This conclusion however, requires validation with an additional refined wind tunnel test.

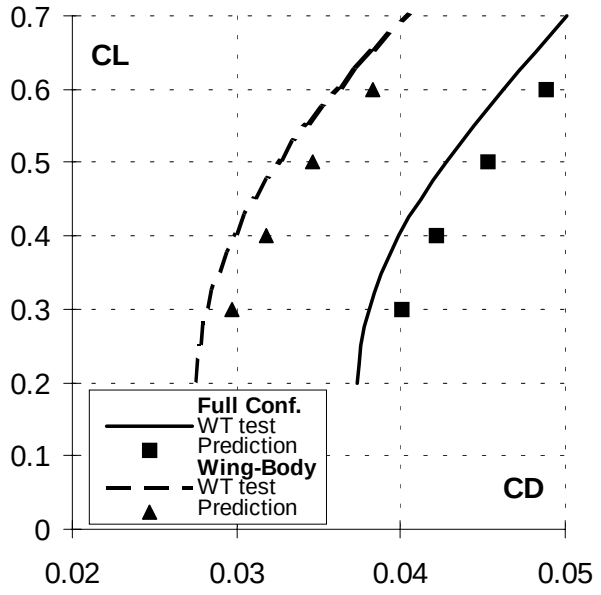

Figure 9: Drag polar from wind tunnel, flap=0^0, comparison to prediction

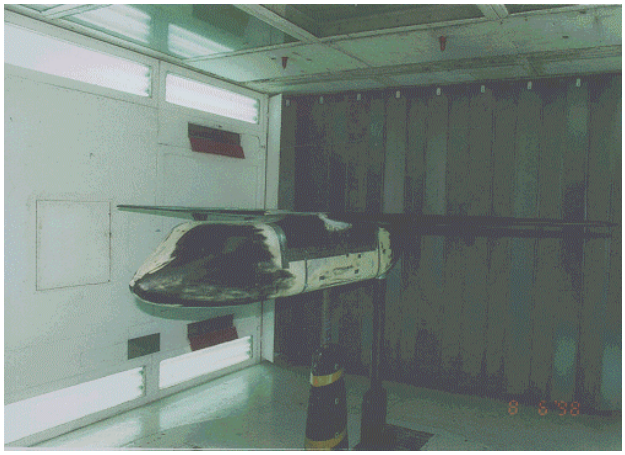

Figure 10: 1:10 Model installation in wind tunnel, central bayonet

3.4 Drag at cruise conditions, and wing size

Cruise at high speed was considered the most demanding point, and therefore the wing area was checked several times during the design.

A formula for a quick check was used for this special case where the following constraints existed: 1. Known aircraft weight 2. Constant fuselage cross section 3. Cruise altitude limited by operational considerations 4. High airspeed specified by mission requirements.

For such conditions the fuselage and tail drag may be considered almost as a constant. To reduce total drag the wing drag component must therefore be minimized.

Since total lift is known (equals weight) the minimum wing drag will be achieved when it has maximum Lift/Drag ratio. Assuming a simple parabolic formula for wings' drag, this will occur when:

$$CLopt = \sqrt{Cdowing * (\pi * e * AR)}$$

Using conditions 3 and 4 wing optimal wing area can be computed.

For medium altitude flight this formula gave rather low optimal wing area which was later increased due to takeoff considerations.

3.5 Drag at takeoff and landing

For takeoff performance, an additional drag component the yaw drag, must be added to the drag polar which was evaluated for symmetrical flight conditions.

In the literature [5] it is stated that the yaw drag for a turboprop aircraft is greater than that for a jet aircraft. This results from the effect of the propeller slipstream on the wing and vertical tail.

The same trend was also found in IAI by comparing flight test results of the "ARAVA" turboprop and the "ASTRA" turbofan aircrafts. Based on this data, a preliminary value of yaw drag was estimated. Further wind tunnel tests with a powered model are planned, and should give better confidence in this drag component.

3.6 Maximum lift

The maximum lift for the cruise configuration was evaluated as previously described from 2-D data and from the spanwise load distribution [Fig. 6]. This was done both for the full scale and for the wind tunnel model (lower Reynolds number). The maximum lift for takeoff and landing configuration was determined using 2-D calculations [Fig. 3] and by empirical method as described in [2].

The untrimmed maximum lift that was measured in the wind tunnel compared quite well with these predictions [Fig. 11].

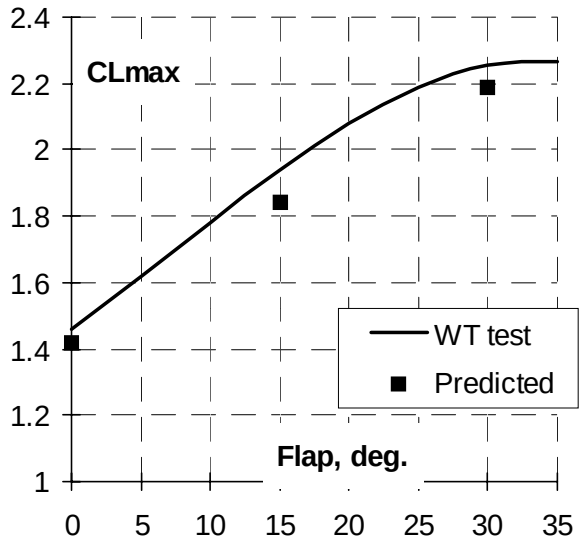

Figure 11: CLmax vs. flap deflection, untrimmed, wind tunnel results, comparison to prediction

4 Stability and Control

4.1 Deep stall

The T-tail configuration was a potential candidate for deep stall phenomena [5].

Results from the wind tunnel [Fig. 12] indicated that deep stall did not occur. This good behavior must still be validated in a wind tunnel test with powered propellers.

In any case, the common use of a stick pusher will eliminate the possibility of a deep stall.

4.2 Directional stability and control

The preliminary sizing of the vertical tail and rudder that was made prior to the wind tunnel test was aimed to achieve adequate Vmc and stability.

Wind tunnel test results confirmed that full rudder deflection was indeed required at $\beta = 0^0$ to ensure adequate Vmc, as predicted. However, for both engines operating, full rudder deflection resulted in very high sideslip angles. Worst case was obtained for landing configuration where it was not possible to trim with full rudder, causing departure in sideslip. The proposed solution was to increase directional stability by either an enlarged tail area or by the addition of ventral fins [Fig. 13].

Tests showed that both solutions are acceptable [Fig. 14]. Other solutions such as limiting the rudder movement in normal flight may also be considered.

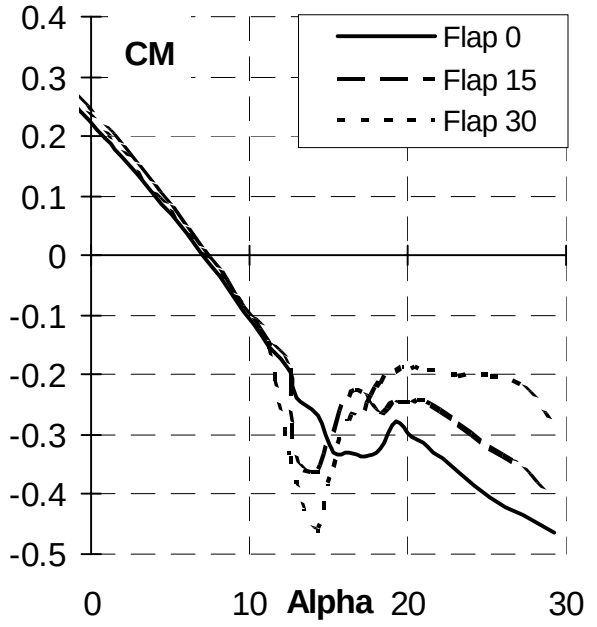

Figure 12: CM vs. α, flap effect, wind tunnel results, aft CG

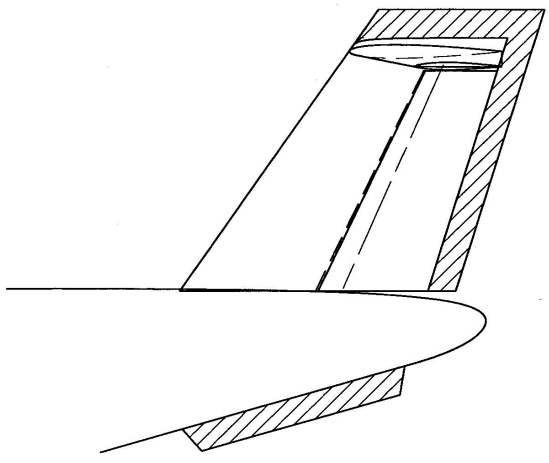

Figure 13: Enlarged vertical tail and ventral fin

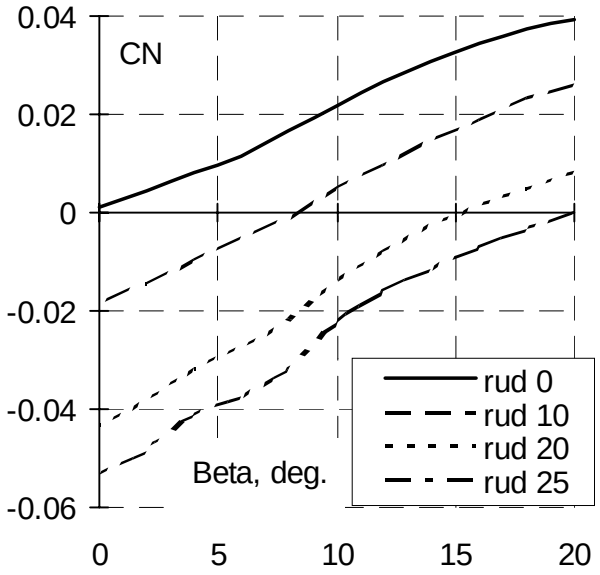

Figure 14: Directional stability and rudder power, wind tunnel results enlarged vertical tail

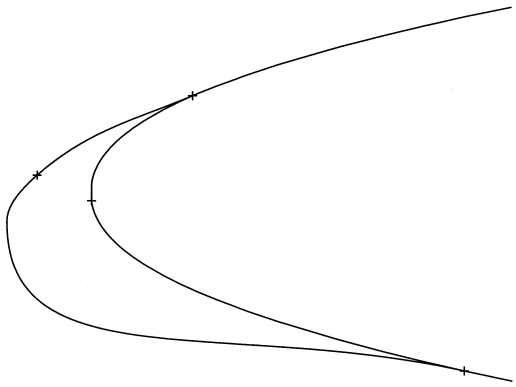

Figure 15: Temporary modification of the leading edge in the wind tunnel model, in the wing-body intersection area

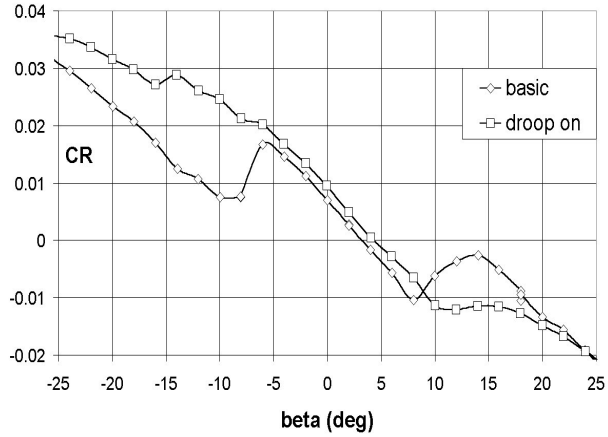

Figure 16: Lateral stability, effect of droop alpha=9.60, flap=300

4.3 Lateral stability

A non-linearity in rolling moment during sideslip was revealed during the wind tunnel test. This was most pronounced at landing configuration and occurred at rather low sideslip angles.

Tuft visualization showed that high local flow inclinations developed on the body side directed toward the flow. This followed by sudden separation on the adjacent inner wing section, causing this non linear rolling moment.

An attempt was made, during the test to add a drooped leading edge in this wing region [Fig. 15]. It showed improved lateral stability [Fig. 16]. However, the droop reduced the pitch down tendency in the stall [Fig. 17].

This solution of wing modification has still to be finalized. Other solutions such as an adequate fairing may be considered.

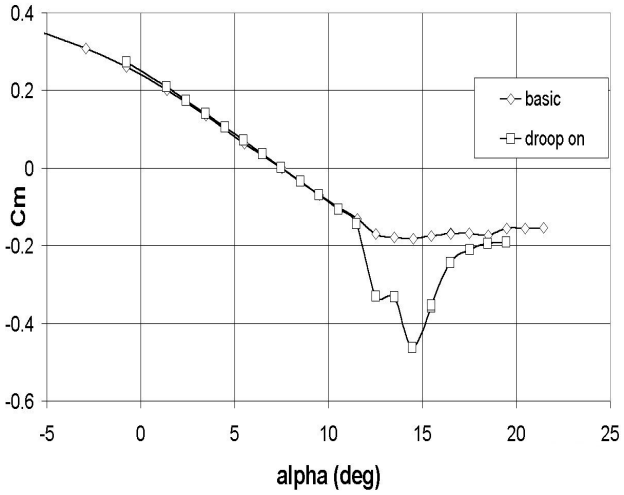

Figure 17: Stall characteristics, effect of droop alpha=9.6^0, flap=30^0

4.4 Power or manual control

At the commencement of preliminary design, manual control of the elevator, rudder and aileron was preferred, taking into account aircraft price.

Manual control of large aircraft requires delicate design of the control devices, large balance ratios, tabs and tailoring for large hinge moments.

Following the design process, it became evident that a full power control of the surfaces is preferable, since this enables lower development costs, and lower development risk and time. It also enables reduction of the gap between the lifting surfaces and the controls, thus reducing the associated drag.

5 Power Effect on Stability and Control

5.1 Basic longitudinal data base

The basic longitudinal characteristics of the aircraft, including lift and moment curves, and elevator power, were estimated using CFD codes [2], and empirical data [6]. This procedure was carried out for different flap positions.

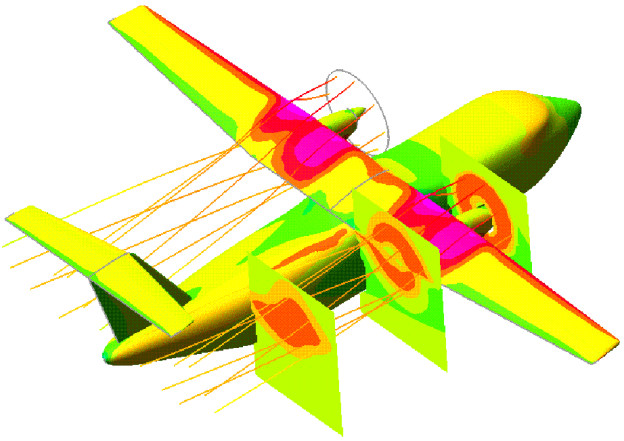

Figure 18: Calculation of power effect, MGAERO, CW propellers

5.2 Longitudinal power effects

The two propellers, mounted before the wing, have a large impact on moments and lift [7]. These changes also depend on the power setting, and cause changes in stability and trim.

The main method to estimate these effects was to use empirical methods [6], [8]. The computations that were carried out were presented as a function of TC, for different flap positions.

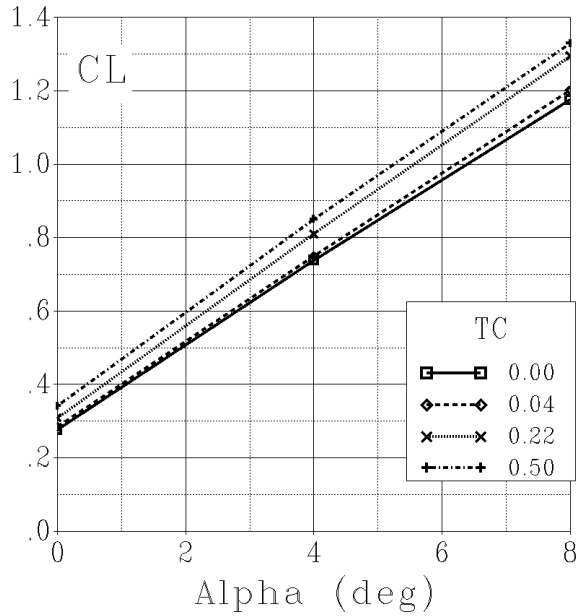

Figure 19: CL vs. α, power effect, MGAERO computation, Mach =0.17, without propeller direct forces

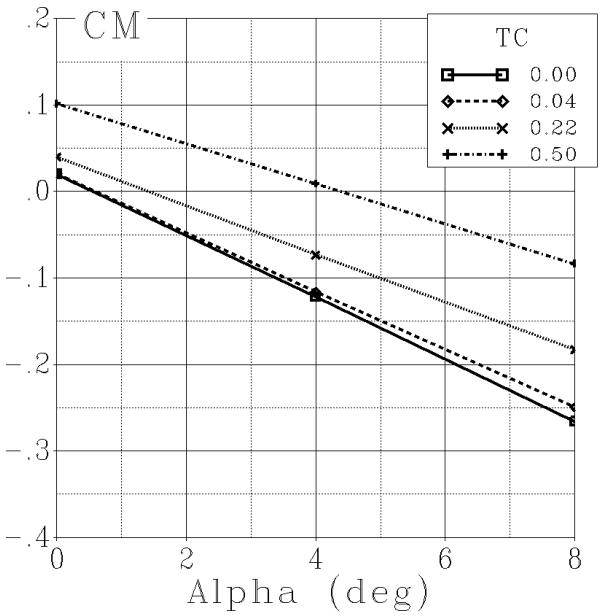

Figure 20: CM vs. α, power effect, MGAERO computation, Mach =0.17, without propeller direct forces

To gain further insight, a computation was carried out with the MGAERO code [2], where its capability to simulate propellers by an

actuator disk and blade element theory was used [Fig. 18].

The computed effect of power on lift and pitching moment is shown [Fig 19], [Fig. 20]. Comparison of neutral point position between computation and empirical methods [Fig. 21] shows that the CFD results reflect the trends of the empirical methods.

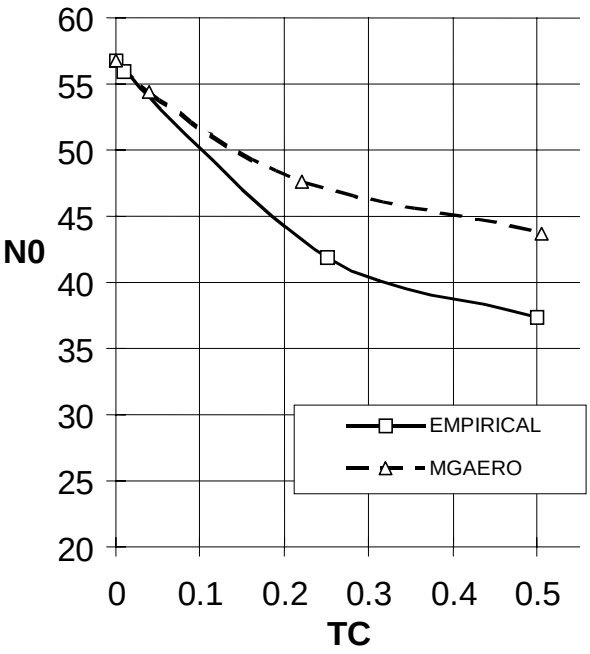

Figure 21: Neutral point vs. TC, comparison of MGAERO and empirical method, without propeller direct forces

6 Summary

The highlights of preliminary aerodynamics design and wind tunnel tests of a cargo transport aircraft were presented. The main goal of this activity was to obtain a higher confidence level in the design goals of the configuration. The cycle of the aerodynamics design followed by three short low speed wind tunnel tests provided the following conclusions.

- Confirmation of drag estimates.
- Maximum lift characteristics as designed.
- Good longitudinal pitching moments, despite T-tail configuration.
- Increase in vertical area and/or incorporation of ventral fins to improve directional characteristics.
- Modification of inner wing leading edge for improvement in lateral stability.

In order to continue validation of this configuration, a power effect wind tunnel test is required during the next phase of activity.

References

[1] MSES, *User's manual.* AMI Redmond Wa. USA

[2] MGAERO, *User's manual.* AMI Redmond Wa. USA

[3] Sherman A. *Interference of wing and fuselage from tests of 30 combinations with triangular and elliptical fuselages in the NACA variable density tunnel.* NACA-TN-1272, May 1947

[4] Ritchie D. J. *Design notes for airplane preliminary design.* AE-420, Jan 1976

[5] Torenbeek E. *Synthesis of subsonic airplane design.* 1982

[6] *USAF Stability and Control Datcom.* 1978

[7] AGARD-CP-160, *Take-off and landing.*

[8] Segall R.N. and Stephanos G. *An enhanced method for reducing power on lift coefficient data to power off lift coefficient data for multi engine propeller aircraft.* AIAA-91-0683, Jan. 1991